Effect of *N*-acetylgalactosamine ligand valency on targeting dendrimers to hepatic cancer cells

Sibu P. Kuruvilla, Gopinath Tiruchinapally, Neha Kaushal, Mohamed E.H. ElSayed

PII: S0378-5173(18)30245-X
DOI: https://doi.org/10.1016/j.ijpharm.2018.04.028
Reference: IJP 17435

To appear in: *International Journal of Pharmaceutics*

Received Date: 15 May 2017
Revised Date: 28 February 2018
Accepted Date: 13 April 2018

Please cite this article as: S.P. Kuruvilla, G. Tiruchinapally, N. Kaushal, M.E.H. ElSayed, Effect of *N*-acetylgalactosamine ligand valency on targeting dendrimers to hepatic cancer cells, *International Journal of Pharmaceutics* (2018), doi: https://doi.org/10.1016/j.ijpharm.2018.04.028

Effect of *N*-acetylgalactosamine ligand valency on targeting dendrimers to hepatic cancer cells

Sibu P. Kuruvilla[1¶], Gopinath Tiruchinapally[2¶*], Neha Kaushal[2], Mohamed E.H. ElSayed[2,3]

[1]Department of Materials Science and Engineering, University of Michigan, Ann Arbor, Michigan, United States of America

[2]Department of Biomedical Engineering, University of Michigan, Ann Arbor, Michigan, United States of America

[3]Program of Macromolecular Science and Engineering, University of Michigan, Ann Arbor, Michigan, United States of America

[¶]These authors contributed equally to this work.

* Corresponding Author:

Gopinath Tiruchinapally, Ph.D.

University of Michigan

Department of Biomedical Engineering

1101 Beal Avenue, 2146 Lurie Biomedical Engineering Building

Ann Arbor, MI 48109, USA

Ph. No. 734-647-2868

E-mail: gtiruchi@umich.edu

Abstract

The display of N-acetylgalactosamine (NAcGal) ligands has shown great potential in improving the targeting of various therapeutic molecules to hepatocellular carcinoma (HCC), a severe disease whose clinical treatment is severely hindered by limitations in delivery of therapeutic cargo. We previously used the display of NAcGal on generation 5 (G5) polyamidoamine (PAMAM) dendrimers connected through a poly(ethylene glycol) (PEG) brush (i.e. G5-*c*PEG-NAcGal; monoGal) to effectively target hepatic cancer cells and deliver a loaded therapeutic cargo. In this study, we were interested to see if tri-valent NAcGal ligands (i.e. $NAcGal_3$) displayed on G5 dendrimers (i.e. G5-*c*PEG-$NAcGal_3$; triGal) could improve their ability to target hepatic cancer cells compared to their monoGal counterparts. We therefore synthesized a library of triGal particles, with either 2, 4, 6, 8, 11, or 14 targeting branches (i.e. *c*PEG-$NAcGal_3$) attached. Conventional flow cytometry studies showed that all particle formulations can label hepatic cancer cells in a concentration-dependent manner, reaching 90-100% of cells labeled at either 285 or 570 nM G5, but interestingly, monoGal labeled more cells at lower concentrations. To elucidate the difference in internalization of monoGal versus triGal conjugates, we turned to multi-spectral imaging flow cytometry and quantified the amount of internalized (I) versus surface-bound (I^0) conjugates to determine the ratio of internalization (I/I^0) in all treatment groups. Results show that regardless of NAcGal valency, or the density of targeting branches, all particles achieve full internalization and diffuse localization throughout the cell ($I/I^0 \sim 3.0$ for all particle compositions). This indicates that while tri-valent NAcGal is a promising technique for targeting nanoparticles to hepatic cancer cells, mono-valent NAcGal is more efficient, contrary to what is observed with small molecules.

Keywords

N-acetylgalactosamine, drug delivery, hepatic cancer cells, poly(amidoamine) (PAMAM) dendrimers, asialoglycoprotein receptor, targeting ligand, monoGal and triGal conjugates

Introduction

Hepatocellular carcinoma (HCC) is the fifth-most commonly occurring tumor worldwide and is the 2nd highest cause for cancer-related deaths. Current treatment procedures involving the delivery of chemotherapy and other small molecule therapies suffer from minimal efficacy and high systemic toxicity due to the lack of targeted drug delivery. Nanotechnology has shown great promise recently to overcome the delivery limitations to localize therapeutic molecules within hepatic cancer tissue. Nanoparticles (NPs) such as synthetic polymers (Kallinteri et al., 2005; Kang et al., 2011; Yoo et al., 2000), natural or metallic materials (Liu et al., 2014), and silica (Li et al., 2010) have all been used to improve the delivery of a variety of payloads to hepatic cancer cells both *in vitro* and *in vivo*, such as siRNA (Wang et al., 2013), imaging dyes (Cao et al., 2015), and small molecule drugs (Kuruvilla et al., 2017; Liu et al., 2014; Scott H Medina et al., 2013). The size characteristics of NPs allow them to passively target tumor tissue by exploiting the enhanced permeation and retention (EPR) effect (Bertrand et al., 2014; Duncan et al., 2013; Fang et al., 2011). Once inside tumor tissue, active targeting of specific molecules improves cellular trafficking of NPs (Arias, 2011; Bertrand et al., 2014).

Targeting the asialogycoprotein receptor (ASGPR), which is specifically overexpressed on hepatic cancer cells (Li et al., 2008; Liu et al., 2014; Trerè et al., 1999) has shown great promise due to its high binding affinity to glycoproteins, which can be synthetically immobilized on a NP

surface to promote highly-efficient binding. We (Kuruvilla et al., 2017; Medina et al., 2011; Scott H. Medina et al., 2013) and others (Lee and Lee, 1997; Rensen et al., 2004; Westerlind et al., 2004) have shown that the display of *N*-acetylgalactosamine (NAcGal) ligands on a NP surface achieves selective internalization into hepatic cancer cells. We showed that mono-valent NAcGal ligands in the β conformation displayed on the tip of a PEG brush attached to generation 5 (G5) poly(amidoamine) (PAMAM) dendrimers (i.e. G5-PEG-NAcGal particles) achieve controllable targeting of hepatic cancer cells (Scott H. Medina et al., 2013). The display of 12-16 moles of PEG-NAcGal branches on the G5 surface (i.e. G5-$(PEG\text{-}NAcGal)_{12\text{-}16}$) enabled efficient delivery of co-loaded drug molecules into the cytoplasm of hepatic cancer cells, improving the therapeutic efficacy of the drug (Kuruvilla et al., 2017).

Interestingly, many studies have shown that the display of multi-valent NAcGal ligands, particularly tri-valent NAcGal (i.e. $NAcGal_3$), improves the ability to target and bind the ASGPR in comparison to mono-valent NAcGal (Khorev et al., 2008; Lee et al., 2011; Nair et al., 2014) in small to medium molecular weight delivery systems. Accordingly, $NAcGal_3$-targeting has successfully been used to deliver molecules like siRNA (Nair et al., 2014) and imaging dyes (Khorev et al., 2008) to hepatic cancer cells, achieving higher intracellular concentrations either at lower delivered concentrations of the therapeutic agent or with improved internalization kinetics. To the best of our knowledge, the efficacy of $NAcGal_3$ targeting has only been studied on small molecules (<13 kDa) and has yet to be investigated for larger molecules such as nanoparticles (>30 kDa). It is important to identify whether the display of $NAcGal_3$ ligands on nanoparticle surfaces can improve their distribution to hepatic cancer cells over mono-valent targeting, similar to what is observed with small molecules.

In this study, we synthesized G5 dendrimers targeted by $NAcGal_3$ ligands attached to the surface through a PEG brush (i.e. G5-[PEG-$(NAcGal_\beta)_3]_n$; **triGal**) and measured their ability to target hepatic cancer cells in comparison to mono-valent G5-$(PEG\text{-}NAcGal)_{12.1}$ conjugates (**Fig 1**). We synthesized a library of **triGal** conjugates with varying density of targeting branches attached, namely with n=2, 4, 6, 8, 11, or 14 moles of PEG-$(NAcGal_\beta)_3$ branches, to achieve **T_2, T_4, T_6, T_8, T_{11}, and T_{14}** conjugates, respectively. We compared the internalization of these particles to that of mono-valent G5-$(PEG\text{-}NAcGal_\beta)_{12.1}$ (**monoGal**; **M_{12}**) conjugates via conventional and multi-spectral imaging flow cytometry methods. Results from this study are useful to understand whether $NAcGal_3$-targeted dendrimers are a viable option to improve nanoparticle-mediated delivery of therapeutic agents to hepatic cancer tissue.

Materials and Methods

Materials

G5-$(NH_2)_{128}$ dendrimers with a diaminobutane core were purchased from Andrews ChemServices (Berrien Springs, MI) and purified by dialysis against deionized water using Slide-A-Lyzer dialysis cassettes (MWCO 10 kDa, Thermo Fisher Scientific, Rockford, IL) to remove imperfect dendrimers and debris. *N*-acetylgalactosamine, pyridine, trimethylphosphine solution (1.0 M in THF), triethylamine (TEA), acetic anhydride (Ac_2O), 1-ethyl-3-(3-dimethylaminopropyl) carbodiimide hydrochloric acid (EDC.HCl), benzotriazol-1-ol (HOBt), trifluoroacetic acid (TFA), anhydrous dimethylsulfoxide (DMSO), anhydrous dichloromethane (DCM), anhydrous dimethylformamide (DMF), anhydrous tetrahydrofuran (THF), anhydrous 1,4-dioxane, *cis*-aconitic anhydride (cis-Ac), alpha bromoacetic acid, sodium hydroxide (NaOH), 10% palladium on activated Carbon (Pd-C), fluorescein isothiocyanate (FITC) sodium methoxide (1.0 M NaOMe solution) and bovine serum albumin (BSA) were purchased from Sigma-Aldrich Inc. (St. Louis, MO). Trimethylsilyl trifluoromethanesulfonate (TMSOTf), N,N-diisopropyl ethyl amine (DIPEA), camphor sulphonic acid (CSA), sodium azide (NaN_3), *N*,*N'*-dicyclohexylcarbodiimide (DCC), ethylacetate (EtOAc), ethanol (EtOH) were purchased from Across Organics Chemicals (Geel, Belgium). N-hydroxysuccinimide-poly(ethylene glycol)-Boc (2 kDa) was purchased from JenKem Technology USA Inc (Plano, TX). 2-{2-(2-Chloroethoxy)ethoxy}ethanol was purchased from TCI America (Portland, OR). Dialysis cassettes (MWCO 1–10 kDa) were purchased from Thermo Fisher Scientific (Rockford, IL). Minimum essential medium (MEM), OPTI-MEM reduced serum medium, fetal bovine serum (FBS), 0.25% trypsin/0.20% ethylenediaminetetraacetic acid (EDTA) solution, phosphate

buffered saline (PBS), penicillin/streptomycin/amphotericin solution, sodium pyruvate, minimum non-essential amino acid (NEAA) solution, and 0.4% trypan blue solutions were purchased from Life Technologies (Thermo Fisher Scientific, Rockford, IL).

Spectral analysis of conjugates

Complete NMR and time-of-flight matrix-assisted laser desorption/ionization (MALDI-TOF) spectra confirming the structural identity and composition of FI_6-G5-*c*PEG-$(NAcGal_\beta)_3$ (**T_2-T_{14}**) conjugates can be found in the **Supporting Information**. Control particles [$(FITC)_6$-G5] and mono-valent FI_6-G5-$[PEG\text{-}NAcGal]_{12.1}$ (**M_{12}**) were synthesized according to our established protocols (Medina et al., 2011; Scott H. Medina et al., 2013). We also synthesized mono-valent FI_6-G5-$[PEG\text{-}NAcGal]_{12.2}$ conjugates with a lysine spacer (**M_{12}-L**) between NAcGal and the PEG branch as a control particle to measure the effect of the spacing structure on cancer cell uptake (**Fig S40**).

Synthesis of FI_6-G5-[*c*PEG-$(NAcGal_\beta)_3]_y$

We chose a similar approach to our previously published strategies to synthesize PEGylated, $(NAcGal_\beta)_3$-targeted G5 conjugates (**Fig 2**) (Medina et al., 2011; Scott H Medina et al., 2013). Briefly, D-N-acetylgalactosamine was treated with Ac_2O and pyridine to obtain D-galactosepentaacetate (**1**), which was treated with TMSOTf in DCM to obtain an oxazolidine derivative (compound **2**). Commercially available 2-(2-(2-chloroethoxy)ethoxy)ethan-1-ol was treated with NaN_3 in DMF to obtain compound **3**. The oxazolidine derivative compound **2**, was

reacted with an alcohol, 2-(2-(2-azidoethoxy)ethoxy)ethan-1-ol (compound **3**) in the presence of D-10-CSA in DMSO at 40 ^{o}C to yield compound **4** having an azide group at the terminal end. The azide functional group of compound **4** was reduced to an amine with Me_3P in THF to obtain compound **5**. Commercially available N6-carbobenzyloxy-L-Lysine was treated with α-bromoacetic acid and NaOH in water at 50°C to obtain compound **6**. The peptide coupling between triacid **6** and the D-galactosamine amine (**5**) was facilitated by DCC, HOBt, and DIPEA in DCM:DMF to obtain a N6-carbobenzyloxy-L-Lysine-$(NAcGal_{\beta})_3$ derivative (**7**) having $(NAcGal_{\beta})_3$ group at one end and Cbz-protected NH_2 on the other end. The carbobenzyloxy (Cbz) group was deprotected by hydrogenolysis under 10% Pd on activated carbon in EtOH/EtOAc at room temperature to obtain 6-NH_2-L-Lysine-$(NAcGal_{\beta})_3$ (**8**), which was reacted with a hetero-functional PEG derivative, (BocNH-PEG-COONHS) in the presence of EDC.HCl, HOBt, and DIPEA in DMF at room temperature to obtain $(NAcGal_{\beta})_3$-L-Lysine-6-NH-PEG-NHBoc (**9**). Acid hydrolysis of compound **9** with TFA:DCM created a Boc-deprotected material $(NAcGal_{\beta})_3$-L-Lysine-6-NH-PEG-NH_2 (**10**), which after reaction with *cis*-aconitic anhydride in H_2O:1,4 dioxane mixture gave a corresponding acid ($(NAcGal_{\beta})_3$-L-Lysine-6-NH-PEG-NH*c*-acid; **11**). These acid functional groups were created to help in coupling them to G5-amine dendrimers. We fluorescently-labeled the G5 dendrimer with fluorescein isothiocyanate (FITC) by treating commercially available G5-$(NH_2)_{128}$ dendrimers with FITC in H_2O:1,4-Dioxane to obtain compound **12** (**Fig 3**). Compound **12** was reacted with different equivalents of ($(NAcGal_{\beta})_3$-L-Lysine-6-NH-PEG-NH*c*-acid (**11**) to obtain a library of conjugates with different targeting ligand concentration on the G5 dendrimer (compounds **13-18**). These coupling reactions were carried out under EDC and HOBt reagents in 6.0 pH phosphate buffer solution. The conjugates were individually reacted with Ac_2O in pyridine to convert the G5 amines into

N-acetyl amines. The materials were then purified by dialysis (10kDa MWCO) and lyophilized to obtain acetylated G5 particles which were further treated with NaOMe in methanol to deprotect the *O*-acetate groups from galactosamine moieties. The reaction mixture was purified by dialysis against deionized water (10kDa MWCO) for 2 days and lyophilized to obtain pure **T_2**: $(FITC)_6$-G5-[*c*PEG-6-NH-Lysine-$(NAcGal_\beta)_3]_2$; **T_4**: $(FITC)_6$-G5-[*c*PEG-6-NH-Lysine-$(NAcGal_\beta)_3]_{3.6}$; **T_6:** $(FITC)_6$-G5-[*c*PEG-6-NH-Lysine-$(NAcGal_\beta)_3]_{5.8}$; **T_8:** $(FITC)_6$-G5-[*c*PEG-6-NH-Lysine-$(NAcGal_\beta)_3]_{8.1}$; **T_{11}:** $(FITC)_6$-G5-[*c*PEG-6-NH-Lysine-$(NAcGal_\beta)_3]_{10.6}$ and **T_{14}:** $(FITC)_6$-G5-[*c*PEG-6-NH-Lysine-$(NAcGal_\beta)_3]_{14.2}$. For clarity purposes, we rounded branch loading to the nearest whole number, and therefore refer to the particles as having either 2, 4, 6, 8, 11, or 14 *c*PEG-$(NAcGal_\beta)_3$ branches attached.

Characterization of triGal conjugates

We measured the particle size of the nanoparticle formulations by dynamic light scattering (DLS) using a 90Plus particle size analyzer (Brookhaven Instruments, Holtsville, NY). The nanoparticles (0.2 mg) were dissolved in 1 mL DI H_20 and tip sonicated using Q500 sonicator for 30 sec. T_2-T_{14} conjugate solutions were then sterile-filtered through syringe filters with a pore size of 0.45 µm and warmed to 37℃ before measurements. Raw distribution data was plotted in Graphpad Prism software and fit using a Gaussian curve, with the mean being taken as the particle size for that replicate. The average of three separate replicates was taken to find the mean particle size ± standard error of the mean (SEM). We also determined the zeta potential of the conjugates using a 90Plus Zeta Potential Analyzer (Brookhaven Instruments, Holtsville, NY).

Particle formulations were dissolved in DI water at 1:20 v/v and warmed to 37℃ before analysis. The average of three separate replicates was taken to find the mean zeta potential ± SEM.

Cell culture

HepG2, Hep3B, and SK-Hep1 cells were cultured in T-75 flasks using MEM supplemented with 10% FBS, 1% antibiotic-antimycotic, 1% sodium pyruvate, 1% non-essential amino acids, and 1 mL gentamicin. HepG2, Hep3B, and SK-Hep1 cells were maintained at 37 ℃, 5% CO_2, and 95% relative humidity and medium was changed every 48 hours. The cells were passaged at 80-90% confluency using a 0.25% trypsin/0.20% EDTA solution.

Uptake of triGal vs. monoGal conjugates into hepatic cancer cells

The internalization of triGal and monoGal conjugates into HepG2, Hep3B, and SK-Hep1 cells was measured as a function of particle composition and concentration via flow cytometry. Briefly, 250,000 HepG2, Hep3B, or SK-Hep1 cells were seeded in 24-well plates and allowed to adhere overnight. Treatment solutions of M_{12}, M_{12}-L, or T_2-T_{14} conjugates (142-570 nM G5 concentration) were prepared in OPTI-MEM and then incubated with the cells for 24 hours at 37 ℃. After removing the treatment medium and washing the cells with warmed PBS twice, the adherent cells were removed from the plates using a 0.25% trypsin/0.20% EDTA solution and then suspended in fresh culture medium. The cells were then transferred to flow cytometry tubes, centrifuged at 1000 RPM for 5 minutes at 4℃, kept on ice, and resuspended immediately before analysis. Samples were analyzed by flow cytometry using the intrinsic fluorescence of FITC (λ_{ex}:

488 nm; λ_{em}: 525 nm) on a Beckman Coulter Cyan ADP instrument provided by the Flow Cytometry Core at the University of Michigan (Ann Arbor, MI). Data is presented as the mean ± SEM for n=4 replicates, and we used untreated cells in blank OPTI-MEM as our negative control. Two-way ANOVA was used to determine the statistical difference between M_{12} and each triGal conjugate at the same concentration (#) and between different concentrations of the same treatment (*) and is denoted by ## or ** for $p<0.01$ and ### or *** for $p<0.001$.

Multi-spectral imaging flow cytometry of triGal vs. monoGal conjugates in hepatic cancer cells

The internalized versus surface-bound ratio of triGal and monoGal conjugates in HepG2 and Hep3B cells was measured using multi-spectral imaging flow cytometry. First, $1x10^6$ HepG2 or Hep3B cells were seeded in 24-well plates and allowed to adhere overnight. Treatment solutions of M_{12} or T_2-T_{14} conjugates at 285 nM G5 concentration were prepared in OPTI-MEM and then incubated with the cells for 24 hours at 37℃. After removing the treatment solution and washing the cells twice with PBS, the adherent cells were removed from the plates using a 0.25% trypsin/0.20% EDTA solution and then suspended in fresh culture medium. The cells were spun down at 1000 RPM at 4℃, the supernatant aspirated, and then resuspended in PBS with 2% FBS at 10^7 cells/mL in microcentrifuge tubes. The cells were then kept on ice and resuspended immediately before analysis. On an Amnis ImagestreamX multi-spectral imaging flow cytometer provided by the Flow Cytometry Core, singular cells in focus were measured for their FITC signal. IDEAS software (EMD Millipore, Billerica, MA) was used to generate two populations of FITC-positive cells based on an internalization ratio determined by the software as a comparison between FITC intensity inside the cell versus the entire cell. We divided the high

internalization group (high internalization ratio, I^0) by the surface-bound group (low internalization ratio, I) in order to quantitatively assess the extent of nanoparticle internalization (I^0/I) between M_{12} and T_2-T_{14} conjugates. I^0/I values are represented as the mean ± SEM of three replicates. We used a one-way ANOVA with Tukey's multiple comparisons test to determine the significance between I^0/I values for each group, with significance being denoted by * for $p<0.05$.

Results and Discussion

We synthesized G5 dendrimers functionalized with a varying density (**n**) of *c*PEG-$(NAcGal_\beta)_3$ branches by modifying our previous synthetic strategies to achieve FITC-labeled G5-[*c*PEG-$(NAcGal_\beta)_3]_n$ conjugates (**Fig 2**) (Kuruvilla et al., 2017; Scott H. Medina et al., 2013). We used the same FITC-labeled G5-NH_2 precursor for monoGal (**M_{12}**) and the library of triGal conjugates (**T_2-T_{14}**) to ensure equivalent fluorescence activity (6 moles of FITC) between each conjugate. We used N6-Cbz-lysine, a known starting material for synthesizing the triGal spacer. (Lee et al., 2011) *N*- alkylation of N6-Cbz-lysine was conducted as described by Du Roure et al. (Du Roure et al., 2003) N6-Cbz-lysine was treated with bromoacetic acid yielded an N6-carbobenzylaxy-L-lysine triacid (**6**), which was coupled to NAcGal-amine (**5**) to obtain compound **7**. The Cbz was deprotected by hydrogenolysis (**8**) and then coupled to a heterofunctional, 2kDa Boc-NH-PEG-NHS ester to obtain compound **9**. After de-protecting the Boc group to establish compound **10**, reaction with *cis*-aconitic anhydride yielded the *c*PEG-$(NAcGal_\beta)_3$ targeting arms (**11**). We coupled compound **11** with the FITC-labeled G5-NH_2 dendrimer (**12**) via peptide coupling at varying molar ratios to achieve **13-18** with different ratios of *c*PEG-$(NAcGal_\beta)_3$ branches attached (**Fig 3**). Finally, the remaining primary G5 amines on these conjugates were acetylated and the *O*-acetyl groups from NAcGal ligands was de-protected to achieve conjugates **T_2-T_{14}**. The conjugates were characterized by ^{1}H-NMR and MALDI for their ligand concentration and molecular weights, which can be found in **Table 1**. We also synthesized monoGal conjugates with the lysine spacer (**M_{12}-L**) to measure the effect of the spacer on cancer cell uptake in comparison to the original **M_{12}** conjugates (**Fig S40**).

The variation in loading of *c*PEG-$(NAcGal_{\beta})_3$ branches corresponded to 1.6, 2.8, 4.5, 6.3, 8.3, and 11.1 mole% PEGylation of **T_2, T_4, T_6, T_8, T_{11}, and T_{14}** conjugates, respectively based on 128 functional primary amines on G5 dendrimer. Given that PEG chains adopt a "mushroom" conformation at low PEG densities (<5 mol%) and switch to a "brush" regime at higher densities, it is expected that T_2-T_{14} conjugates should have differing PEG conformations based on their varying PEG density. PEG chains attached to spherical nanoparticles in the brush conformation typically impart higher hydrodynamic diameters (HD) to the nanoparticles, due to the thin, bristle-like extension of the PEG away from the nanoparticle surface. Conversely, nanoparticles with PEG in the mushroom conformation typically have smaller HDs due to the coiling of the PEG chains. We performed dynamic light scattering (DLS) to identify the HD of triGal conjugates and found that all conjugates exhibit an HD of approximately 7-8 nm, with no statistical significance between them (**Table 1**). This suggests that the differences in PEGylation between T_2-T_{14} conjugates that confers different PEG conformations does not impart significant impacts on the HD of NPs at the nanometer scale.

All conjugates exhibited a size profile that confers the ability to surpass renal filtration from the blood (HD < 5nm (Choi et al., 2009; Longmire et al., 2008)), thereby extending their retention time within the bloodstream. MALDI analysis confirmed that the molecular weight (MW) of triGal particles increased with increasing density of *c*PEG-$(NAcGal_{\beta})_3$ branches (**Table 1**). It is important to note that both T_2 and T_4 conjugates (34,725 and 39,789 Da, respectively) fall under the MW cut-off (40,000 Da) estimated to enable nanoparticles to exploit the EPR effect (Duncan et al., 2013; Maeda et al., 2009; Seki et al., 2009). Studies in tumor-bearing mice will help identify whether these conjugates are retained within the bloodstream and cleared through the

urine before they can concentrate into tumor tissue. T_6-T_{14}, however, have MWs that should enable their easy exploitation of the EPR effect. Finally, we measured the zeta potential of T_2-T_{14} conjugates and confirmed that they are neutral (**Table 1**), which should prevent non-specific charge-charge interactions (Sadekar and Ghandehari, 2013) and protein opsonization (Alexis et al., 2008) while circulating in the bloodstream.

Table 1: Physicochemical Properties of G5-[*c*PEG-$(NAcGal_\beta)_x]_n$

Particle Type	Graphical Depiction	Chemical Structure	# of *c*PEG-$(NAcGal_\beta)_x$ branches (n)	Total $NAcGal_\beta$ loading per G5	Molecular Weight (Da)	Particle Size (nm)	Zeta Potential (mV)
monoGal (x=1)	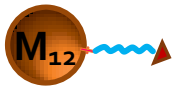	$(FITC)_6$-**G5**-[*c*PEG-$NAcGal_\beta]_{12}$	12	12.1	59,171	7.4 ± 0.30	-0.30 ± 0.21
triGal (x=3)	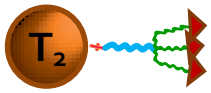	$(FITC)_6$-**G5**-[*c*PEG-$(NAcGal_\beta)_3]_2$	2	5.2	34,275	8.3 ± 1.4	-4.6 ± 0.28
	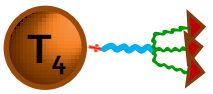	$(FITC)_6$-**G5**-[*c*PEG-$(NAcGal_\beta)_3]_4$	4	11.0	39,789	7.7 ± 0.2	0.0 ± 0.0
	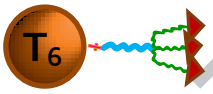	$(FITC)_6$-**G5**-[*c*PEG-$(NAcGal_\beta)_3]_6$	6	18.0	47,230	7.5 ± 1.0	-1.5 ± 1.6
	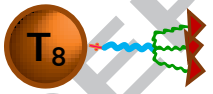	$(FITC)_6$-**G5**-[*c*PEG-$(NAcGal_\beta)_3]_8$	8	23.4	55,256	6.8 ± 1.0	0.0 ± 0.0
		$(FITC)_6$-**G5**-[*c*PEG-$(NAcGal_\beta)_3]_{11}$	11	25.5	63,863	7.5 ± 0.97	0.0 ± 0.0
	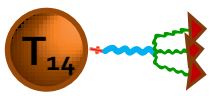	$(FITC)_6$-**G5**-[*c*PEG-$(NAcGal_\beta)_3]_{14}$	14	41.4	76,221	8.6 ± 0.30	0.0 ± 0.0

Uptake of triGal vs. monoGal in hepatic cancer cells

We used flow cytometry to establish whether the library of triGal conjugates could be recognized and internalized by hepatic cancer cells, and to identify how this internalization compared to that of monoGal conjugates. Briefly, we incubated M_{12} and T_2-T_{14} conjugates at 142, 285, and 570 nM G5 concentration with either HepG2, Hep3B, or SK-Hep1 cells for 24 hours. Data for Hep3B and SK-Hep1 cells can be found in supplementary **Fig S57** and **S58**, respectively. We previously established that the internalization of G5-based conjugates targeted by monoGal ligands are internalized by hepatic cancer cells at a $NAcGal_\beta$ concentration range of 100-4000 nM (Kuruvilla et al., 2017; Medina et al., 2011; Scott H. Medina et al., 2013). With 12-16 moles of *c*PEG-$NAcGal_\beta$ attached to the dendrimers, these concentrations corresponded 7-285 nM of G5 dendrimers. At 142 and 285 nM G5, we achieve 100% uptake into HepG2 and Hep3B cells with monoGal-targeted particles (M_{12}). Correspondingly we chose a concentration range of 142-570 nM in this study to compare the internalization of monoGal versus triGal conjugates into HepG2 and Hep3B cells. Results show that T_2-T_{14} conjugates label HepG2 in a concentration-dependent manner, labeling only 2-4% of HepG2 cells at 142 nM G5 but reaching 100% cell labeling at 570 nM (**Fig 4**). Interestingly, at a low concentration of 142 nM, M_{12} labels 8- to 15-fold more cells than any of the triGal conjugates, reaching strong statistical significance between it and all triGal conjugates ($p<0.0001$, M_{12} vs. T_2-T_{14}). At 285 nM, the labeling of HepG2 cells by T_2-T_{14} conjugates increases significantly (64-89% cells labeled). Of particular note, T_8, T_{11}, and T_{14} conjugates achieve higher cell labeling (89, 89 and 85%, respectively) than T_2, T_4, and T_6 (64, 72, 72%, respectively) with statistical significance ($p<0.01$ for all comparisons). Importantly, M_{12} labels virtually all cells (99%) with statistically significant differences from all triGal conjugates ($p<0.001$). At this concentration of G5, the $NAcGal_\beta$ present on M_{12} conjugates

(3420 nM) falls in between that displayed by T_{11} (3135 nM) and T_{14} (3990 nM) conjugates. Regardless, M_{12} achieves statistically higher labeling of cells above both of T_{11} and T_{14} (89 and 85% of cells, respectively). At the highest concentration of 570 nM G5, all conjugates label 100% of cells. We conducted similar uptake studies in another ASGPR-positive hepatic cancer cell line, Hep3B, and found similar results **(Fig S57**). Further, we investigated the uptake of triGal and monoGal conjugates in SK-Hep1 cells, an ASGPR-deficient HCC cell line (Saxena et al., 2002; Tai et al., 2012), to ensure that the uptake was mediated and dependent on this receptor (**Fig S58**). For all particles, there was less than <10% internalization into SK-Hep1 cells at all concentrations after 24 hours, verifying that internalization for both M_{12} and T_2-T_{14} conjugates is ASGPR-mediated. Additionally, to ensure the difference in uptake between M_{12} and T_2-T_{14} conjugates is not due to the lysine spacer included in the T_2-T_{14} conjugates, we synthesized a lysine-based monoGal, M_{12}-L, and showed that it exhibits no difference in uptake into HepG2 cells compared to M_{12} conjugates in this concentration range (**Fig S49**). We therefore conclude that the presence of the spacer does not affect hepatic cancer cell uptake of NAcGal-targeted dendrimers and is not the reason for differences between M_{12} and T_2-T_{14} labeling.

Taken together, our results show that triGal conjugates are ASGPR-specific and able to label 100% HepG2 cells at the highest concentrations, while at lower concentrations they achieve cell labeling but to a lower extent. However, M_{12} conjugates label 1.5-8 folds more HepG2 cells at lower G5 concentrations (i.e 142-285 nM), suggesting that mono-valent NAcGal$_\beta$-targeting of G5 dendrimers is more efficient at being recognized by hepatic cancer cells.

Surface versus internal localization of triGal vs monoGal in HepG2 cells

Given our initial flow cytometry results, we sought to understand why triGal conjugates, while being able to label HepG2 cells, cannot do so as efficiently as their monoGal counterparts despite similar concentrations of $NAcGal_{\beta}$. We hypothesized that the decrease in cell labeling may come from one of a few theories related to valency-dependent cell-binding. In particular, many investigators have described receptor cross-linking using coiled-coil networks, which describes molecules targeting a receptor at the cell surface that are connected to a larger polymer network (i.e. coiled-coil), creating a crosslinking of receptors through this extracellular network and rendering them deficient or even sometimes leading to apoptosis induction (Wu et al., 2010; Zacco et al., 2015). We hypothesized that triGal conjugates could be inducing a similar "receptor crosslinking" phenomenon. This would be possible if the same *c*PEG-$(NAcGal_{\beta})_3$ branch was bound to multiple ASGPRs, where both would "pull" on the same NP for endocytosis, but face competition by an equal and opposite force from another engaged receptor. In this way, the G5 dendrimer would be the "network" causing the receptor crosslinking, and while triGal conjugates would be bound to the cell surface they may not be internalized fully. This would help explain why other investigators (Khorev et al., 2008; Lee et al., 2011; Nair et al., 2014) have observed that triGal-targeted small molecules exhibit improved distribution to hepatic cancer cells, but when triGal is attached to larger molecules (e.g. nanoparticles), the geometry complicates the binding and internalization potential.

To distinguish between surface-bound and internalized nanoparticles, we turned to multi-spectral imaging flow cytometry, which adds the ability to microscopically image cells being sorted by flow cytometry in order to identify the cellular localization of the fluorescence, and in this case, the nanoparticles (Phanse et al., 2012). We incubated either M_{12} or T_2-T_{14} conjugates at 285 nM for 24 hours with HepG2 (**Fig 5**) and for Hep3B (**Fig S59**) cells and used the data collection software to measure the internalization ratio of each FITC-labeled cell and separate them into cells with surface-bound nanoparticles or cells with mostly internalized ones. It is important to note that these two populations are presented as a percentage of all FITC-labeled cells, so differences in cell labeling mentioned above are accounted for in this analysis and are not relevant. Results indicate that the localization of nanoparticles does not differ between triGal and monoGal conjugates, and also does not differ between the triGal conjugates themselves. Images collected for all treatments during flow cytometry show both punctate fluorescence at cell membranes, indicating surface-bound nanoparticles, and diffuse fluorescence within the cell indicating nanoparticle diffusion throughout the cell body.

We also quantitatively evaluated the extent of internalization for all nanoparticle treatments by determining I^0/I, a metric comparing the extent of nanoparticle internalization (I^0) versus surface localization (I) HepG2 (**Fig 6**) and for Hep3B (**Fig S60**). $I^0/I > 1$ would indicate higher internalization than surface-bound localization, while $I^0/I < 1$ would indicate higher surface localization than internalization. Results show that I^0/I ranged from 3.2 for T_2 conjugates up to 4.1 for T_8 conjugates, with no statistical significance between any of the treatment groups. This indicates that there was significantly higher internalization than surface localization for all treatments. Further, the lack of difference in I^0/I values between triGal and monoGal conjugates

indicates that there are in fact no higher surface-localized triGal conjugates than there are monoGal conjugates. Since these populations contain an equivalent number of cells that are labeled by the NPs, the equivalence in internalized versus surface-bound particles between monoGal and triGal treatments indicates that the internalization kinetics are similar between the two.

Our earlier results showing that monoGal labels more cells than triGal suggests that the differences in valency contribute to the kinetics of receptor binding, but not of internalization once the particles are bound to the ASGPR. We believe therefore that receptor-crosslinking may not be occurring with triGal conjugates. It is possible that the geometric spacing between $NAcGal_{\beta}$ ligands at the tip of *c*PEG-$(NAcGal_{\beta})_3$ branches affects their kinetics of binding to the ASGPR. Khorev *et al.* showed through molecular modeling that the length of the flexible spacer attaching $NAcGal_{\beta}$ ligands to the backbone as well as the space between each $NAcGal_{\beta}$ ligand specifically impacted their binding affinity to ASGPR (Khorev et al., 2008). Zacco *et al.* built off of this work to create a glycopeptide library studying various combinations of spacer lengths and distances between $NAcGal_{\beta}$ ligands, identifying that $NAcGal_{\beta}$ ligands spaced 7 amino acids from each other on a peptide backbone and at the tip of an 18 angstrom spacer achieved the best targeting of the ASGPR (Zacco et al., 2015). While these conditions were all established by testing triGal ligands either incubated alone or attached to small molecules, we believe the specific geometric requirements will be even more important when triGal ligands are attached to nanoparticles. In fact, with multiple triGal branches attached to the same nanoparticle, as is the case in the present study, further complications may arise from steric hindrance, repulsion, and competitive binding. Hence the discrepancy we are observing between triGal targeting of

nanoparticles versus previously established targeting of small molecules. We are currently undertaking molecular modeling and geometric measurements of our triGal library to help elucidate these differences. Nevertheless, this study suggests that the display of triGal branches on G5 dendrimers does not improve internalization kinetics compared to the display of monoGal ligands, as was the phenomenon observed for small molecules. However, the triGal conjugates presented here still provide a library of potential drug delivery vehicles that can be used for hepatic cancer therapy, depending on the constraints of fabrication, therapeutic loading, and biodistribution.

Conclusions

This study focuses on the synthesis and validation of a library of G5 dendrimers displaying a varying density (n=2, 4, 6, 8, 11, or 14) of tri-valent $(NAcGal_{\beta})_3$ ligands as potential drug delivery vehicles for hepatic cancer therapy. Our results indicate that triGal conjugates achieve concentration-dependent internalization into hepatic cancer cells that is comparable to our-previously established mono-valent, $NAcGal_{\beta}$-targeted dendrimers. Interestingly, triGal conjugates do not exhibit improved internalization over monoGal conjugates, as was observed previously with triGal-targeting of small molecules. In fact, monoGal conjugates more efficiently label hepatic cancer cells than triGal conjugates at lower concentrations. Further, multi-spectral imaging flow cytometry confirmed that the localization of triGal conjugates is both intracellular and at the surface, similar to their monoGal counterparts. Taken together, it is evident that binding of G5 dendrimers to the ASGPR is affected by NAcGal valency, but the process of how they are internalized is less susceptible to the difference. To the best of our

knowledge, this is the first study to describe the effect of multi-valent $NAcGal_{\beta}$ ligands on nanoparticle targeting of hepatic cancer cells. The synthetic strategies, biological findings, and library of conjugates established in this work offers information crucial to improving drug delivery strategies for the treatment of hepatic cancer.

Acknowledgments

S.P.K. and G.T. contributed equally to this work. The authors would like to thank Dr. Jinsang Kim for providing access to their fluorescence spectrophotometer instrument. Sibu P. Kuruvilla recognizes the support of the NSF Graduate Research Fellowship (GRFP) award and the University of Michigan Rackham Merit Fellowship (RMF).

References

Alexis, F., Pridgen, E., Molnar, L.K., Farokhzad, O.C., 2008. Factors Affecting the Clearance and Biodistribution of Polymeric Nanoparticles. Mol. Pharm. 5, 505–515.

Arias, J.L., 2011. Drug targeting strategies in cancer treatment: an overview. Mini Rev. Med. Chem. 11, 1–17. doi:10.2174/138955711793564024

Bertrand, N., Wu, J., Xu, X., Kamaly, N., Farokhzad, O.C., 2014. Cancer nanotechnology: The impact of passive and active targeting in the era of modern cancer biology. Adv. Drug Deliv. Rev. 66, 2–25. doi:10.1016/j.addr.2013.11.009

Cao, Y., He, Y., Liu, H., Luo, Y., Shen, M., Xia, J., Shi, X., 2015. Targeted CT imaging of human hepatocellular carcinoma using low-generation dendrimer-entrapped gold nanoparticles modified with lactobionic acid. J. Mater. Chem. B 3, 286–295. doi:10.1039/C4TB01542H

Choi, H.S., Liu, W., Misra, P., Tanaka, E., Zimmer, J.P., Itty, B., Bawendi, M.G., Frangioni, J. V, 2009. Renal Clearance of Nanoparticles. Nat. Biotechnol. 25, 1165–1170. doi:10.1038/nbt1340.Renal

Du Roure, O., Debiemme-Chouvy, C., Malthête, J., Silberzan, P., 2003. Functionalizing surfaces with nickel ions for the grafting of proteins. Langmuir 19, 4138–4143. doi:10.1021/la020636z

Duncan, R., Sat-Klopsch, Y.-N., Burger, A.M., Bibby, M.C., Fiebig, H.H., Sausville, E. a, 2013. Validation of tumour models for use in anticancer nanomedicine evaluation: the EPR effect and cathepsin B-mediated drug release rate. Cancer Chemother. Pharmacol. 72, 417–427. doi:10.1007/s00280-013-2209-7

Fang, J., Nakamura, H., Maeda, H., 2011. EPR effect: the unique characteristics of tumor blood vessels for drug delivery, factors involved, its limitation and augmentation. Adv. Drug Deliv. Rev. 63, 136–151.

Kallinteri, P., Higgins, S., Hutcheon, G. a, St Pourçain, C.B., Garnett, M.C., 2005. Novel functionalized biodegradable polymers for nanoparticle drug delivery systems. Biomacromolecules 6, 1885–94. doi:10.1021/bm049200j

Kang, Y.M., Kim, G.H., Kim, J. Il, Kim, D.Y., Lee, B.N., Yoon, S.M., Kim, J.H., Kim, M.S., 2011. In vivo efficacy of an intratumorally injected in situ-forming doxorubicin/poly(ethylene glycol)-b-polycaprolactone diblock copolymer. Biomaterials 32, 4556–4564. doi:10.1016/j.biomaterials.2011.03.007

Khorev, O., Stokmaier, D., Schwardt, O., Cutting, B., Ernst, B., 2008. Trivalent, Gal/GalNAc-containing ligands designed for the asialoglycoprotein receptor. Bioorg. Med. Chem. 16, 5216–31. doi:10.1016/j.bmc.2008.03.017

Kuruvilla, S.P., Tiruchinapally, G., ElAzzouny, M., ElSayed, M.E.H., 2017. N-Acetylgalactosamine-Targeted Delivery of Dendrimer-Doxorubicin Conjugates Influences Doxorubicin Cytotoxicity and Metabolic Profile in Hepatic Cancer Cells. Adv. Healthc. Mater. 6, 1601046. doi:10.1002/adhm.201601046

Lee, R.T., Lee, Y.C., 1997. Facile Synthesis of a High-Affinity Ligand for Mammalian Hepatic Lectin Containing Three Terminal N-Acetylgalactosamine Residues. Bioconjug. Chem. 8, 762–765. doi:10.1021/bc9700796

Lee, R.T., Wang, M.-H., Lin, W.-J., Lee, Y.C., 2011. New and more efficient multivalent glyco-ligands for asialoglycoprotein receptor of mammalian hepatocytes. Bioorg. Med. Chem. 19, 2494–500. doi:10.1016/j.bmc.2011.03.027

Li, L., Tang, F., Liu, H., Liu, T., Hao, N., Chen, D., Teng, X., He, J., 2010. In vivo delivery of silica nanorattle encapsulated docetaxel for liver cancer therapy with low toxicity and high efficacy. ACS Nano 4, 6874–6882.

Li, Y., Huang, G., Diakur, J., Wiebe, L.I., 2008. Targeted Delivery of Macromolecular Drugs: Asialoglycoprotein Receptor (ASGPR) Expression by Selected Hepatoma Cell Lines used in Antiviral Drug Development. Curr. Drug Deliv. 5, 299–302. doi:10.2174/156720108785915069

Liu, H., Wang, H., Xu, Y., Guo, R., Wen, S., Huang, Y., Liu, W., Shen, M., Zhao, J., Zhang, G., Shi, X., 2014. Lactobionic acid-modified dendrimer-entrapped gold nanoparticles for targeted computed tomography imaging of human hepatocellular carcinoma. ACS Appl. Mater. Interfaces 6, 6944–53. doi:10.1021/am500761x

Longmire, M., Choyke, P.L., Kobayashi, H., 2008. Clearance Properties of Nano-sized Particles and Molecules as Imaging Agents: Considerations and Caveats. Nanomedicine 3, 703–717. doi:10.2217/17435889.3.5.703.Clearance

Maeda, H., Bharate, G.Y., Daruwalla, J., 2009. Polymeric drugs for efficient tumor-targeted drug delivery based on EPR-effect. Eur. J. Pharm. Biopharm. 71, 409–419.

Medina, S.H., Chevliakov, M. V, Tiruchinapally, G., Durmaz, Y.Y., Kuruvilla, S.P., Elsayed, M.E.H., 2013. Enzyme-activated nanoconjugates for tunable release of doxorubicin in hepatic cancer cells. Biomaterials 34, 4655–4666. doi:10.1016/j.biomaterials.2013.02.070

Medina, S.H., Tekumalla, V., Chevliakov, M. V, Shewach, D.S., Ensminger, W.D., El-Sayed, M.E.H., 2011. N-acetylgalactosamine-functionalized dendrimers as hepatic cancer cell-targeted carriers. Biomaterials 32, 4118–4129. doi:10.1016/j.biomaterials.2010.11.068

Medina, S.H., Tiruchinapally, G., Chevliakov, M. V., Durmaz, Y.Y., Stender, R.N., Ensminger, W.D., Shewach, D.S., ElSayed, M.E.H., 2013. Targeting Hepatic Cancer Cells with PEGylated Dendrimers Displaying N- Acetylgalactosamine and SP94 Peptide Ligands. Adv. Healthc. Mater. 2, 1337–1350. doi:10.1002/adhm.201200406

Nair, J.K., Willoughby, J.L.S., Chan, A., Charisse, K., Alam, M.R., Wang, Q., Hoekstra, M., Kandasamy, P., Kelin, A. V., Milstein, S., Taneja, N., Oshea, J., Shaikh, S., Zhang, L., Van Der Sluis, R.J., Jung, M.E., Akinc, A., Hutabarat, R., Kuchimanchi, S., Fitzgerald, K., Zimmermann, T., Van Berkel, T.J.C., Maier, M.A., Rajeev, K.G., Manoharan, M., 2014. Multivalent N -acetylgalactosamine-conjugated siRNA localizes in hepatocytes and elicits robust RNAi-mediated gene silencing. J. Am. Chem. Soc. 136, 16958–16961. doi:10.1021/ja505986a

Phanse, Y., Ramer-Tait, A.E., Friend, S.L., Carrillo-Conde, B., Lueth, P., Oster, C.J., Phillips, G.J., Narasimhan, B., Wannemuehler, M.J., Bellaire, B.H., 2012. Analyzing cellular internalization of nanoparticles and bacteria by multi-spectral imaging flow cytometry. J. Vis. Exp. e3884. doi:10.3791/3884

Rensen, P.C.N., van Leeuwen, S.H., Sliedregt, L.A.J.M., van Berkel, T.J.C., Biessen, E.A.L., 2004. Design and Synthesis of Novel N-Acetylgalactosamine-Terminated Glycolipids for Targeting of Lipoproteins to the Hepatic Asialoglycoprotein Receptor. J. Med. Chem. 47, 5798–5808. doi:10.1021/jm049481d

Sadekar, S., Ghandehari, H., 2013. Transepithelial Transport and Toxicity of PAMAM Dendrimers: Implications for Oral Drug Delivery. Adv. Drug Deliv. Rev. 64, 571–588. doi:10.1016/j.addr.2011.09.010.TRANSEPITHELIAL

Saxena, A., Yik, J.H.N., Weigel, P.H., 2002. H2, the minor subunit of the human asialoglycoprotein receptor, trafficks intracellularly and forms homo-oligomers, but does not bind asialo-orosomucoid. J. Biol. Chem. 277, 35297–35304. doi:10.1074/jbc.M205653200

Seki, T., Fang, J., Maeda, H., 2009. Tumor-targeted macromolecular drug delivery based on the enhanced permeability and retention effect in solid tumor, in: Lu, Y., Mahato, R. (Eds.), Pharmaceutical Perspectives of Cancer Therapeutics. Springer Science & Business Media, p. 100.

Tai, W.-T., Cheng, A.-L., Shiau, C.-W., Liu, C.-Y., Ko, C.-H., Lin, M.-W., Chen, P.-J., Chen,

K.-F., 2012. Dovitinib induces apoptosis and overcomes sorafenib resistance in hepatocellular carcinoma through SHP-1-mediated inhibition of STAT3. Mol. Cancer Ther. 11, 452–63. doi:10.1158/1535-7163.MCT-11-0412

Trerè, D., Fiume, L., De Giorgi, L.B., Di Stefano, G., Migaldi, M., Derenzini, M., 1999. The asialoglycoprotein receptor in human hepatocellular carcinomas: its expression on proliferating cells. Br. J. Cancer 81, 404–8. doi:10.1038/sj.bjc.6690708

Wang, H.-X., Xiong, M.-H., Wang, Y.-C., Zhu, J., Wang, J., 2013. N-acetylgalactosamine functionalized mixed micellar nanoparticles for targeted delivery of siRNA to liver. J. Control. Release 166, 106–14. doi:10.1016/j.jconrel.2012.12.017

Westerlind, U., Westman, J., Törnquist, E., Smith, C.I., Oscarson, S., Lahmann, M., Norberg, T., 2004. Ligands of the asialoglycoprotein receptor for targeted gene delivery, part 1: synthesis of and binding studies with biotinylated cluster glycosides containing N-acetylgalactosamine. Glycoconjugate J. 21, 227–241.

Wu, K., Liu, J., Johnson, R.N., Yang, J., Kopecek, J., 2010. Drug-Free Macromolecular Therapeutics: Induction of Apoptosis by Coiled-Coil-Mediated Cross-Linking of Antigens on the Cell Surface. Angew. Chemie 49, 1451–1455.

Yoo, H.S., Lee, K.H., Oh, J.E., Park, T.G., 2000. In vitro and in vivo anti-tumor activities of nanoparticles based on doxorubicin-PLGA conjugates. J. Control. Release 68, 419–431. doi:10.1016/S0168-3659(00)00280-7

Zacco, E., Hütter, J., Heier, J.L., Mortier, J., Seeberger, P.H., Lepenies, B., Koksch, B., 2015. Tailored Presentation of Carbohydrates on a Coiled Coil-Based Scaffold for Asialoglycoprotein Receptor Targeting. ACS Chem. Biol. 10, 2065–2072. doi:10.1021/acschembio.5b00435

Fig 1: Strategy for multi-valent targeting of hepatic cancer cells. We compared the effect of tri-valent NAcGal display on targeting G5 dendrimers to hepatic cancer cells in comparison to mono-valent NAcGal. We attached $NAcGal_3$ ligands attached to the G5 surface through a PEG brush and a cis-aconitic spacer (*c*) to achieve G5-(*c*PEG-$NAcGal_3)_n$ (i.e. **triGal**) conjugates and compared their distribution to hepatic cancer cells to mono-valent G5-(*c*PEG-$NAcGal)_{12.1}$ (i.e. **monoGal**) conjugates. We synthesized a library of triGal conjugates with varying density of targeting branches attached, namely with n=2, 4, 6, 8, 11, or 14 moles of PEG-$NAcGal_3$ branches, to achieve T_2, T_4, T_6, T_8, T_{11}, and T_{14} conjugates, respectively. We compared the internalization of monoGal and triGal conjugates via conventional and multi-spectral imaging flow cytometry methods.

Fig 2: Synthesis of $(NAcGal_\beta)_3$-Lysine-6-NH-PEG-NH_2 (10)

Fig 3: Synthesis of T_2-T_{14} conjugates

Fig 4: Uptake of triGal vs. monoGal into HepG2 cells. We measured the uptake of monoGal and triGal conjugates into HepG2 cells via flow cytometry. M_{12}, T_2, T_4, T_6, T_8, T_{11}, and T_{14} conjugates were incubated at G5 concentrations of 142, 285, and 570 nM, which corresponded to various $NAcGal_\beta$ concentrations based on the loading density, as seen in the table. Results show that both monoGal and triGal label HepG2 cells with increasing concentration, with monoGal achieving higher labeling at lower conjugate concentrations. T_2, T_4, and T_6 exhibited lower internalization than T_8, T_{11}, and T_{14} conjugates, likely due to their loaded $NAcGal_\beta$ differences. Results are presented as the mean of four replicates ± SEM. Two-way ANOVA was used to determine the statistical difference M_{12} and each triGal conjugate at the same concentration (#) and between different concentrations of the same treatment (*), and is denoted by # or * for $p<0.05$, ## or ** for $p<0.01$, and ### or *** for $p<0.001$.

Fig 5: Surface versus internalized localization of monoGal and triGal conjugates in HepG2 cells. We used multi-spectral imaging flow cytometry to visualize surface-bound conjugates and internalized conjugates, as assessed by an IDEAS software-based internalization algorithm. Results show that monoGal and triGal conjugates achieve both surface-localization and internalization after 24 hour incubation at 285 G5 nM.

Fig 6: Internalized versus surface bound ratio (I^0/I) of T_2-T_{14} and M_{12} conjugates in HepG2 cells. We quantitatively assessed the ratio of FITC-labeled HepG2 cells with high internalization (I^0) versus low internalization (I) by determining I^0/I. Results show that for all treatment groups, the conjugates were internalized to a much greater extent than they were maintained at the surface, as indicated by I^0/I values > 1. Further, the I^0/I values between monoGal and triGal

conjugates are not statistically different, indicating that they achieve the same ratio of internalized particles when they label cells. Results are presented as the mean of three replicates ± SEM. A one-way ANOVA test was used to determine differences between each conjugate group.

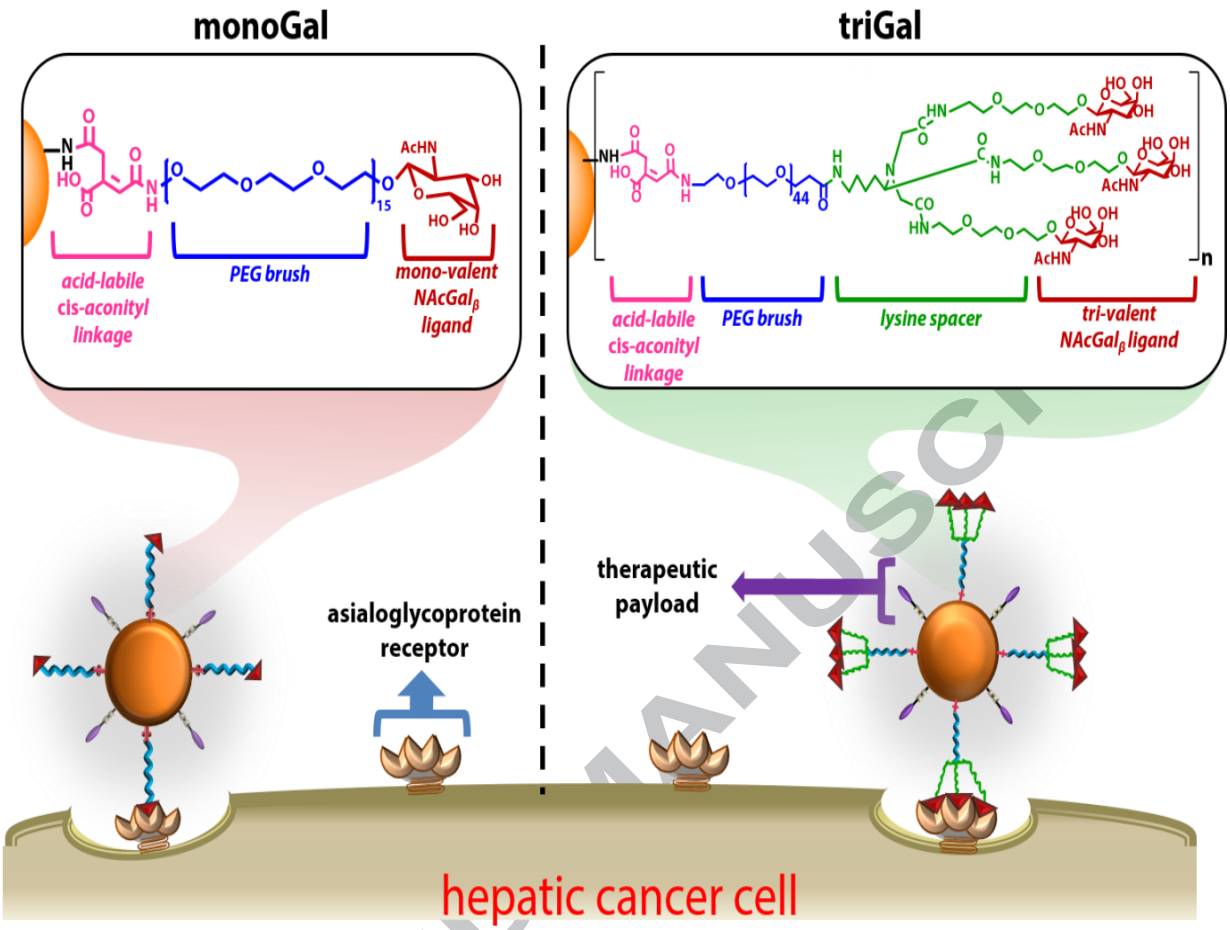

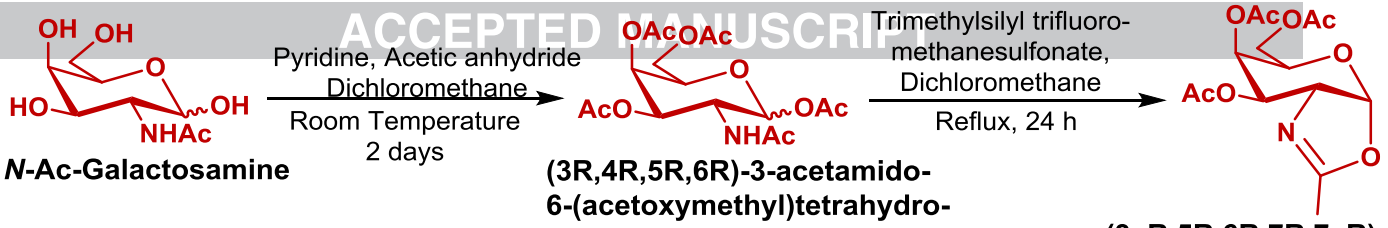

***N*-Ac-Galactosamine**

(3R,4R,5R,6R)-3-acetamido-6-(acetoxymethyl)tetrahydro-2H-pyran-2,4,5-triyl triacetate
(**1**)

(3aR,5R,6R,7R,7aR)-5-(ac
methyl)-2-methyl-3a,6,7,7
tetrahydro-5H-pyrano-[3,2
oxazole-6,7-diyl diacetate
(**2**)

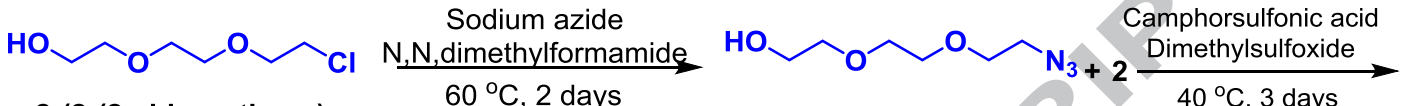

2-(2-(2-chloroethoxy)ethoxy)ethan-1-ol

2-(2-(2-azidoethoxy)ethoxy)ethan-1-ol
(**3**)

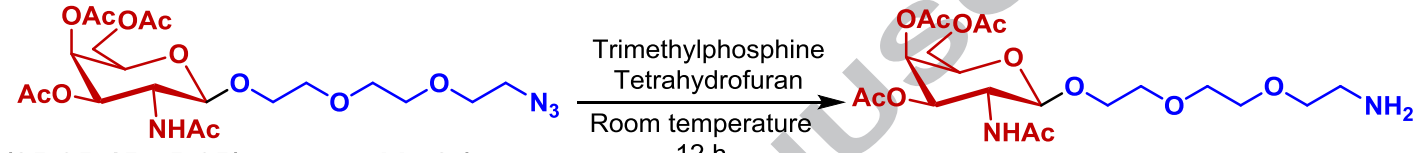

(2*R*,3*R*,4*R*,5*R*,6*R*)-5-acetamido-2-(acetoxymethyl)-6-(2-(2-azidoethoxy)ethoxy)ethoxy)tetrahydro-2*H*-pyran-3,4-diyl diacetate
(**4**)

(2*R*,3*R*,4*R*,5*R*,6*R*)-5-acetamido-2-(acetoxymethyl)-6-(2-(2-(2-aminoethoxy)ethoxy)ethoxy)tetrahydro-2*H*-pyran-3,4-diyl diacetate
(**5; NAcGal**)

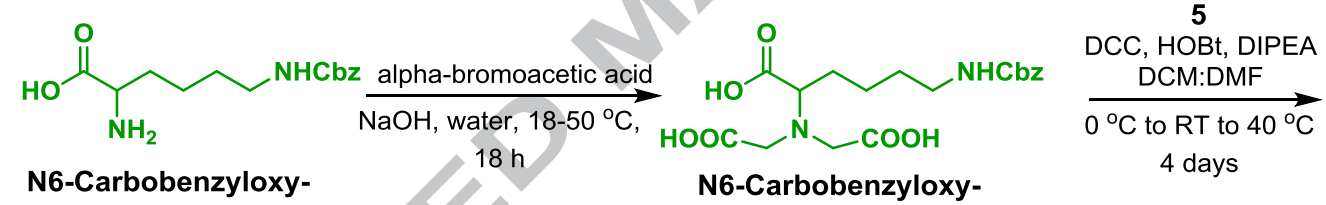

N6-Carbobenzyloxy-L-Lysine

N6-Carbobenzyloxy-L-Lysine-tri-acetic acid
(**6**)

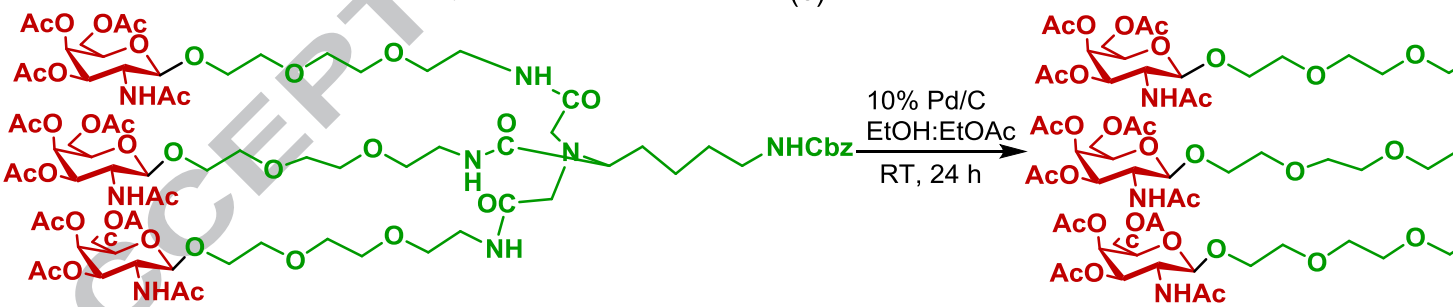

(7; N6-Carbobenzyloxy-L-Lysine-(NAcGal$_\beta$)$_3$)

(8; 6-NH$_2$-L-Lysine-(NAcGal$_\beta$)$_3$

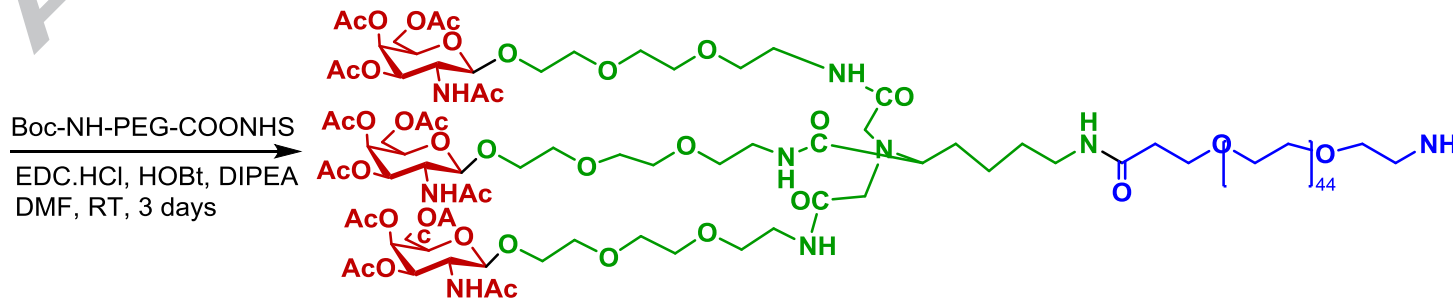

(9; (NAcGal$_\beta$)$_3$-Lysine-6-NH-PEG-NHBoc

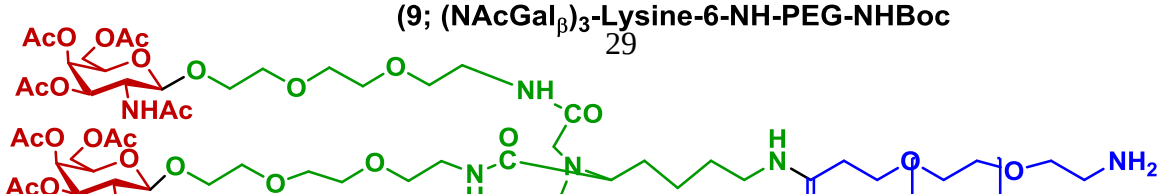

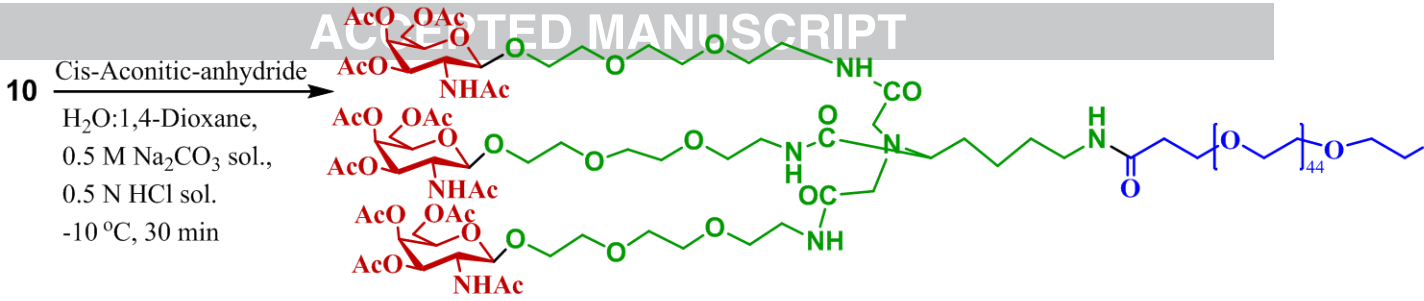

(11; $(NAcGal_\beta)_3$-Lysine-6-NH-PEG*c*-acid

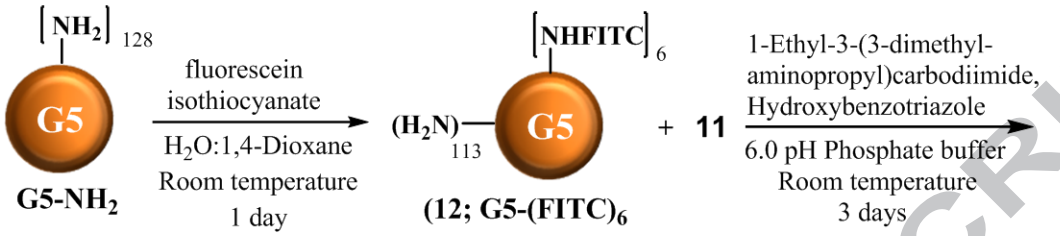

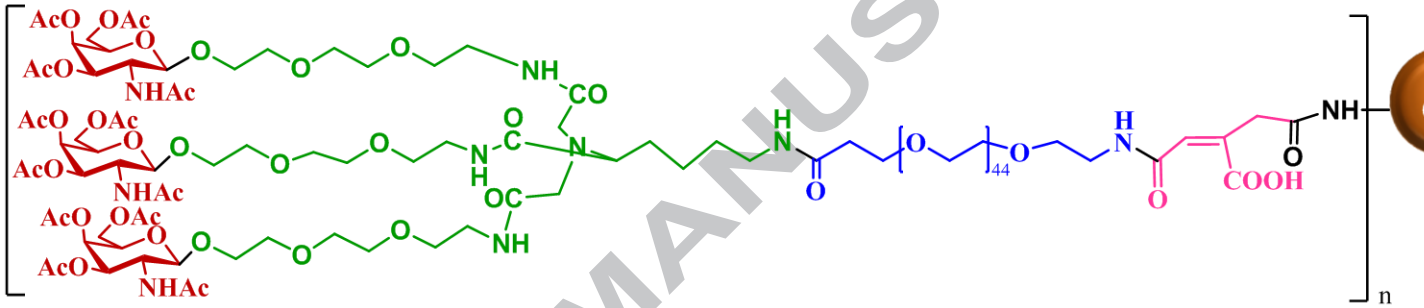

(13; n = 2; $(FITC)_6$-G5-[*c*PEG-6-NH-Lysine-$(NAcGal_\beta$-Ac)$_3]_2$
(14; n = 3.6; $(FITC)_6$-G5-[*c*PEG-6-NH-Lysine-$(NAcGal_\beta$-Ac)$_3]_{3.6}$
(15; n = 5.8; $(FITC)_6$-G5-[*c*PEG-6-NH-Lysine-$(NAcGal_\beta$-Ac)$_3]_{5.8}$
(16; n = 8.1; $(FITC)_6$-G5-[*c*PEG-6-NH-Lysine-$(NAcGal_\beta$-Ac)$_3]_{8.1}$
(17; n = 10.6; $(FITC)_6$-G5-[*c*PEG-6-NH-Lysine-$(NAcGal_\beta$-Ac)$_3]_{10.6}$
(18; n = 14.2; $(FITC)_6$-G5-[*c*PEG-6-NH-Lysine-$(NAcGal_\beta$-Ac)$_3]_{14.2}$

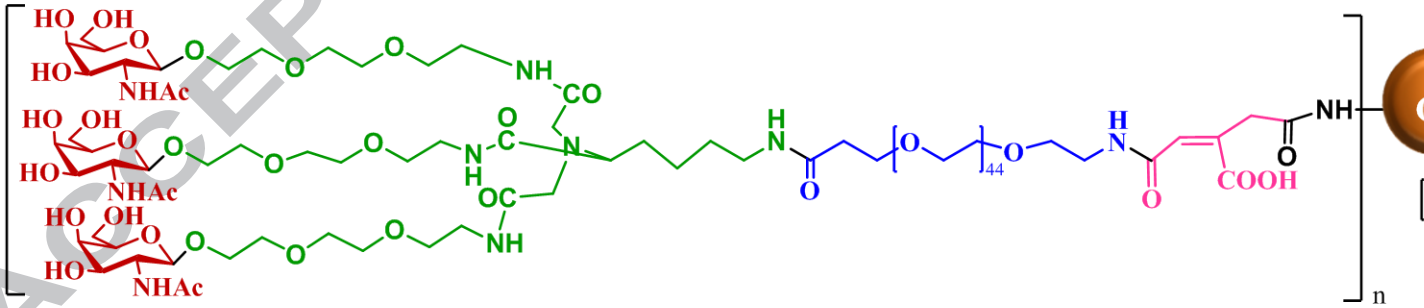

(T_2; n = 2; $(FITC)_6$-G5-[*c*PEG-6-NH-Lysine-$(NAcGal_\beta)_3]_2$
(T_4; n = 3.6; $(FITC)_6$-G5-[*c*PEG-6-NH-Lysine-$(NAcGal_\beta)_3]_{3.6}$
(T_6; n = 5.8; $(FITC)_6$-G5-[*c*PEG-6-NH-Lysine-$(NAcGal_\beta)_3]_{5.8}$
(T_8; n = 8.1; $(FITC)_6$-G5-[*c*PEG-6-NH-Lysine-$(NAcGal_\beta)_3]_{8.1}$
(T_{11}; n = 10.6; $(FITC)_6$-G5-[*c*PEG-6-NH-Lysine-$(NAcGal_\beta)_3]_{10.6}$
(T_{14}; n = 14.2; $(FITC)_6$-G5-[*c*PEG-6-NH-Lysine-$(NAcGal_\beta)_3]_{14.2}$

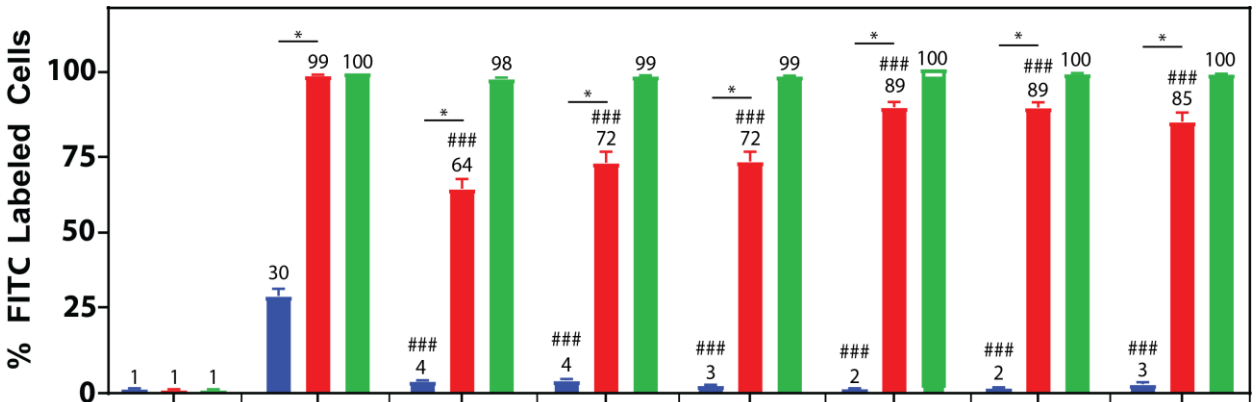

G5 conc'n	Control	M12	T2	T4	T6	T8	T11	T14
142 nM		1704	852	1704	2556	3408	4686	5964
285 nM		3420	1710	3420	5130	6840	9405	11,970
570 nM		6840	3420	6840	10,260	13,680	18,810	23,940

Equivalent NAcGal Concentration (nM)

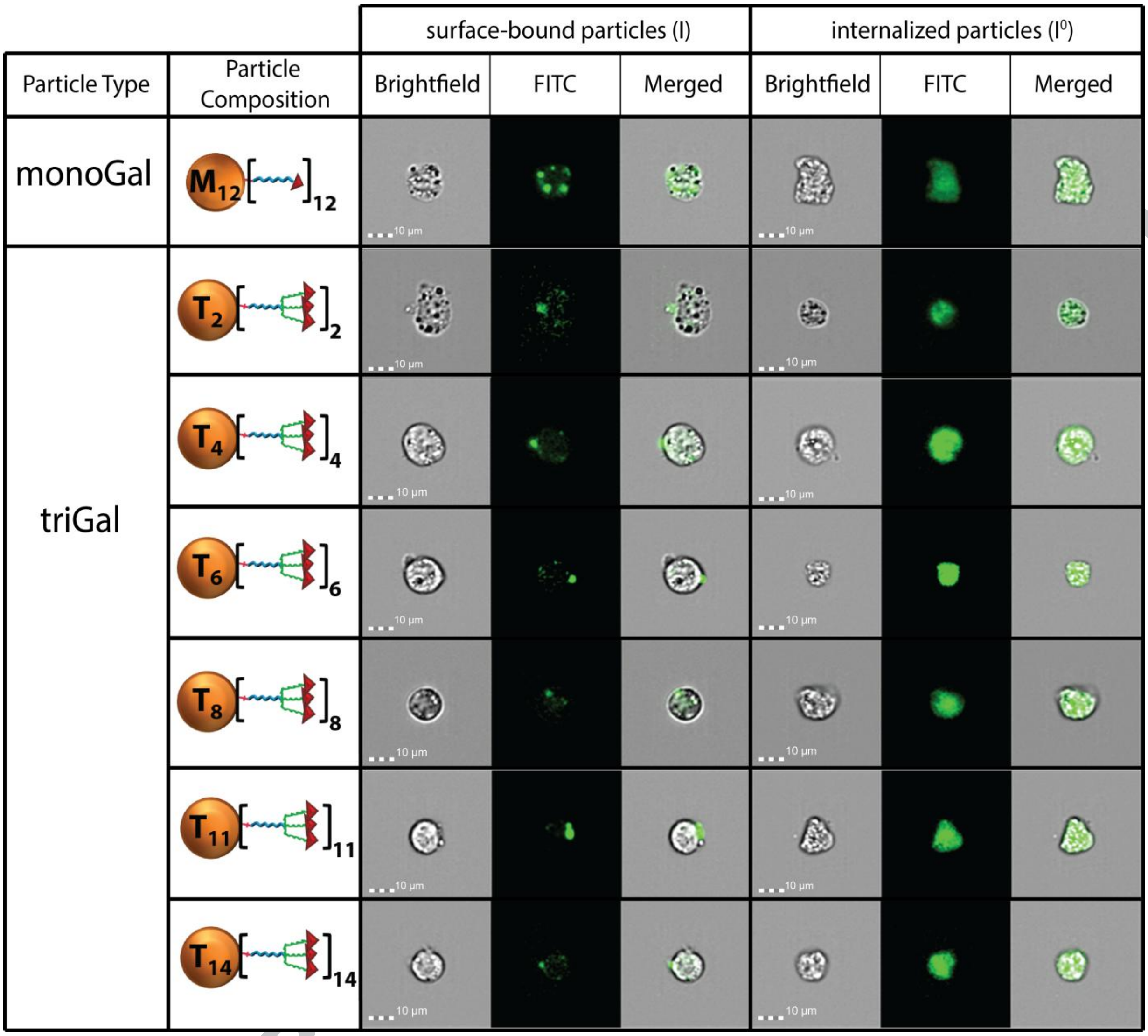

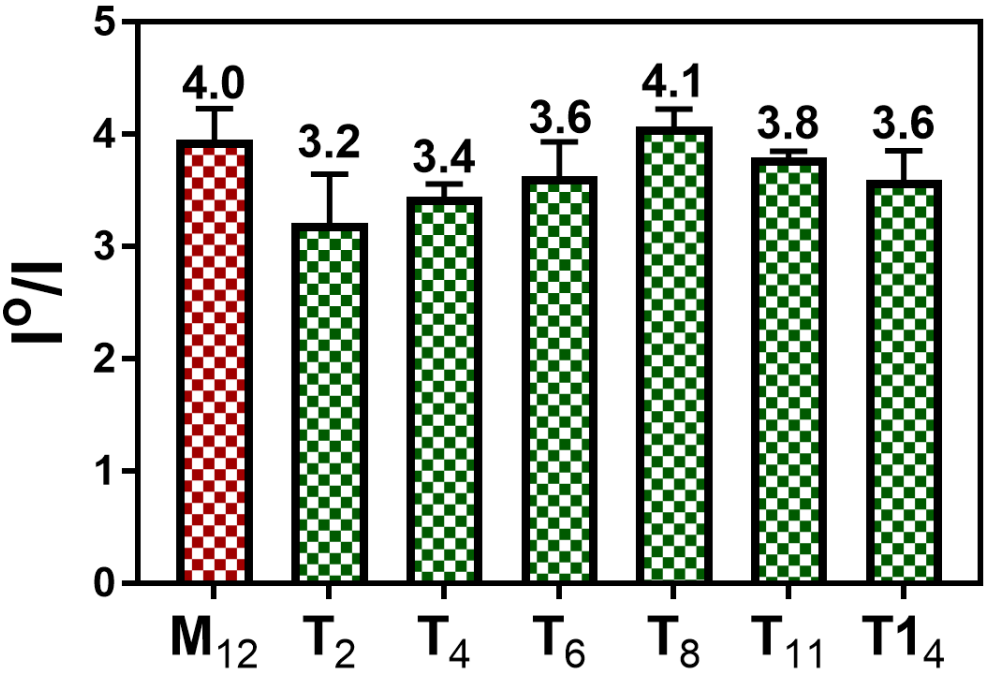

Graphical abstract